

Probing the Ultrastructure of Spheroids and Their Uptake of Magnetic Nanoparticles by FIB–SEM

Original

Probing the Ultrastructure of Spheroids and Their Uptake of Magnetic Nanoparticles by FIB–SEM / Mollo, V.; Scognamiglio, P.; Marino, A.; Ciofani, G.; Santoro, F.. - In: ADVANCED MATERIALS TECHNOLOGIES. - ISSN 2365-709X. - STAMPA. - 5:3(2020), p. 1900687. [10.1002/admt.201900687]

Availability:

This version is available at: 11583/2801883 since: 2020-03-11T11:22:15Z

Publisher:

Wiley-Blackwell

Published

DOI:10.1002/admt.201900687

Terms of use:

openAccess

This article is made available under terms and conditions as specified in the corresponding bibliographic description in the repository

Publisher copyright

Wiley postprint/Author's Accepted Manuscript

This is the peer reviewed version of the above quoted article, which has been published in final form at <http://dx.doi.org/10.1002/admt.201900687>. This article may be used for non-commercial purposes in accordance with Wiley Terms and Conditions for Use of Self-Archived Versions.

(Article begins on next page)

1 **Probing the ultrastructure of spheroids and their uptake of**
2 **magnetic nanoparticles by FIB-SEM**

3 Valentina Mollo^{1±}, Paola Scognamiglio^{1±}, Attilio Marino², Gianni Ciofani^{2,3}, Francesca Santoro^{1*}

4
5 ¹Center for Advanced Biomaterials for Healthcare, Istituto Italiano di Tecnologia, Naples, Italy.

6 ²Smart Bio-Interfaces, Istituto Italiano di Tecnologia, Pontedera, Italy.

7 ³Department of Mechanical and Aerospace Engineering, Politecnico di Torino, Torino, Italy.

8
9 *Correspondence to: francesca.santoro@iit.it

10
11 [±]these authors have equal contribution.

12
13
14
15
16 **MANUSCRIPT**
17

18 **Abstract**

19 Spheroids are 3D cellular systems largely adopted as model for high-throughput screening of
20 molecules and diagnostics tools. Furthermore, those cellular platforms also represent a model for
21 testing new delivery carries for selective targeting. The coupling between the 3D cell environment
22 and the nanovectors can be explored at the macroscale by optical microscopy. However, the
23 nanomaterial-cell interplay finds major action at the single cell and extracellular matrix level with
24 nanoscale interactions. Electron microscopy offers the resolution to investigate those interactions,
25 however the specimen preparation finds major drawbacks in its operation time and preciseness. In
26 this context, focused ion beam and scanning electron microscopy (FIB-SEM) allows for fast
27 processing and high resolution of the cell-nanomaterial interface. Here, in fact, we show a novel
28 approach to prepare large-area 3D spheroid cell culture specimens for FIB-SEM. We explored
29 sectioning procedures to preserve the peculiar structure of spheroids and their interaction with
30 magnetic nanovectors. Our results pave the way for advanced investigations of 3D cellular systems
31 with nano and micromaterials relevant to tissue engineering, bioelectronics and diagnostics.

32

33 **Keywords:** scanning electron microscopy, focused ion beam, spheroids, biointerfaces,
34 nanocarriers, endocytosis.

35

36 **Introduction**

37 In the last decade, spheroid-like cellular architectures have become powerful model systems to
38 biomimic complex tissue-like forms towards the fully recapitulation of organoid-like systems. In
39 fact, these closed-systems are excellent tools for understanding complex cellular functions, testing
40 new molecules for drugs and diagnostics solutions^[1]. In this context, 3D tumor spheroids have
41 been adopted as reliable model of *in vivo* solid tumors for the screening of different anticancer
42 drugs and nanoformulations^[2,3]. In comparison to 2D cancer cell cultures, tumor spheroids display
43 many different features of the *in vivo* solid tumors (*e.g.*, spatial architecture, high-level secretion
44 of soluble mediators, gene expression profile and multidrug resistance mechanisms)^[4].

45 Our former studies, for instance, adopted spheroid-like tumoral system to evaluate the efficacy of
46 lipid nanovectors have been loaded with superparamagnetic iron oxide nanoparticles (SPIONs)^[5].
47 SPIONs efficiently generate heat when exposed to alternated magnetic fields (AMF) and have
48 been successfully exploited for hyperthermia treatment of glioblastoma in clinical trials^[6].

49 Furthermore, our group has recently developed lipid nanovectors loaded with both SPIONs and
50 the temozolomide (TMZ) drug for the combined hyperthermia and chemotherapy treatment of
51 glioblastoma cells^[7]. For all these aforementioned applications (i.e. hyperthermia, MRI imaging
52 and chemotherapy treatment), the nanovector accumulation inside the 3D tumor models is of
53 crucial importance.

54 In this scenario, these 3D closed- systems and their interaction with nanomaterials have been so
55 far largely investigated by means of optical microscopy techniques^[8,9]. However, there are
56 certainly limitations in terms of characterization of the inner spheroid interactions, achieved
57 resolution and labelling of multiple cellular components. Alternatively, 3D cell architectures can
58 be further inspected at the nanoscale by electron microscopy techniques. In fact, the typical
59 polymeric embedding ensures that the 3D morphology is preserved and the cross sectioning allows
60 for the investigation of specific thin sections and eventually the reconstruction of a volume of
61 interest^[10].

62 Transmission electron microscopy can be performed following a mechanical thin-sectioning,
63 allowing for slice thickness in the range of ~ 70 nm^[11]. Given the large size of 3D spheroids, this
64 procedure would yield to hundreds of sections which might be collected and analyzed individually.
65 This is an extremely time consuming process and recently, scanning electron microscopy coupled
66 with in-chamber mechanical serial sectioning tools have provided an alternative approach for fast
67 processing and imaging ^[12].

68 Here, serial block-face imaging scanning electron microscopy (SBF-SEM) and focus ion beam
69 scanning electron microscopy (FIB-SEM) found major applications for morphological analysis of
70 stem cell spheroids, organoids, as well as organotypic cell cultures.

71 SBF-SEM uses the automated ultramicrotome located inside the SEM chamber and removes
72 sections (≥ 20 nm thick) from the block face and provides scanning of relatively large volumes.

73 Alternatively, focused ion beam- scanning electron microscopy (FIB-SEM) tomography is the
74 most promising approach for 3D imaging at the subcellular level and is considered as a revolution
75 for ultrastructural volume reconstruction^[13–15] avoiding the drawbacks of mechanical sectioning
76 procedures and achieving sections' thickness < 20 nm. In fact, this technique has been already
77 adopted for the investigation of 2D and 3D cultures on diverse biomaterials^[16–19] and the
78 characterization of complex tissue-like architectures.^[20,21]

79 In this work, we further exploit the FIB-SEM procedure to investigate regions of interest in 3D
80 spheroid cell cultures and their interaction with magnetic nanovectors, which can penetrate and
81 reach the spheroid inner domain. The spheroids have been macroscopically observed employing
82 two specimens preparation procedures which include hard drying and resin-embedding processes.
83 Given the large size of the spheroids, those have been initially mechanically sectioned to reduce
84 their effective volume and be subsequently polished by focused ion beam. Finally, we characterize
85 the interface between cell and extracellular matrix with magnetic nanovectors exploring the
86 different phases of the SPIONs uptake process.

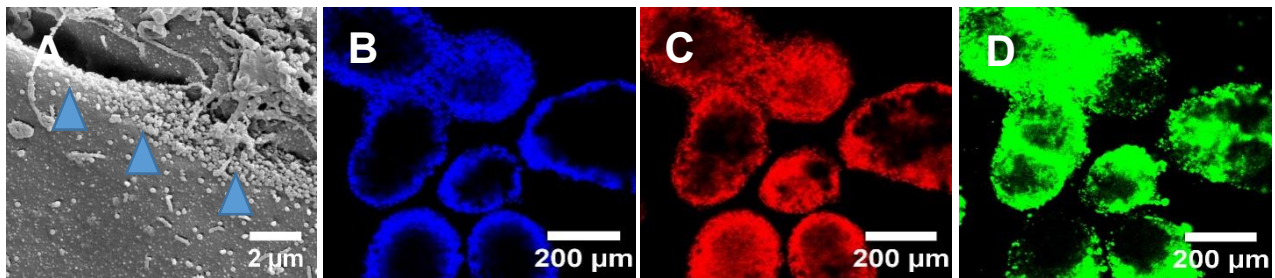
87

88 **Results**

89 3D spheroids have been obtained from U87 MG cells and assemble in a 3D architecture following
90 the hanging-drop procedure (see **Experimental Section**). The U87 MG-derived spheroids were
91 loaded with lipid magnetic nanovectors (LMNVs) labeled with a lipophilic fluorescent probe,
92 which marked the lipid part of the vectors (24-48 hours of incubation). Nanovectors approach the
93 surface of individual cells (**Figure 1A**, the scanning electron micrograph of spheroid also shows
94 the interaction of LMNVs with its surface as shown by the blue arrows) and they further penetrate
95 both in the intracellular and inter-cellular domains. In fact, **Figure 1B-D** show how cells and
96 nanovectors simultaneously populate the spheroids.

97 Thus, through fluorescence imaging, the rate of penetration and the quantification of LMNVs
98 inside the spheroids were calculated. In fact, after 24 hours 0.8 % (s.d.: +- 0.7 %) of the total
99 volume of the spheroids were populated by LMNVs and after 48 hours this volume reaches 8.1%
100 (s.d.:+- 0.5 %)^[5]. To further evaluate the nanovector-spheroid interface interaction, we prepared
101 the specimens for SEM/FIB milling and imaging.

102



103

104 **Figure 1: Morphology of U87_MG derived spheroids and nanovector internalization: A)**

105 Scanning electron micrograph of spheroid surface treated with ROTO protocol with lipid magnetic

106 nanovectors, LMNVs (blue arrow). B,C,D) confocal laser scanning microscopy imaging of
107 spheroids: nuclei in blue (Hoechst) with fluorescent nanovectors in green and F-actin in red; scan
108 area is 1273 μm x 1273 μm .

109
110 Due to the large size, sectioning *via* FIB of a whole spheroid (400-500 μm) would require
111 extremely long processing times. For this reason, each spheroid was divided in to four parts during
112 the fixation and embedding procedure. The cutting was carried out carefully with a small razor
113 blade (see **Supplementary Information S1**). To assess the possible damages due to the
114 mechanical sectioning (i.e. compression, breakages, eradication of organelles, etc.), the
115 ultrastructure of the spheroids was investigated after each step of cutting.

116 The ROTO-UTP (reduced osmium–thiocarbohydrazide–osmium ultra thin plasticization) protocol
117 used for the specimen preparation is structured in nine main steps (**Figure 2**, Box A), in relation
118 to the use of different substances for fixation and heavy-metal staining (glutaraldehyde, glycine,
119 osmium tetroxide/potassium ferro-cyanide, thiocarbohydrazide, osmium tetroxide, uranyl acetate,
120 tannic acid, ethanol, Spurr’s resin). Among these procedure’s steps, six were selected as a point in
121 time when each spheroid was sliced in to four parts. Thus, we identify six cutting steps: step 1: after
122 fixation in glutaraldehyde; step 2: after osmium tetroxide; step 3: after thiocarbohydrazide (TCH);
123 step 4: after tannic acid; step 5: in resin embedding before polymerization; step 6: in resin after
124 polymerization as described in **Figure 2 (Box A-B)**. After each cutting step, the each spheroid
125 section was embedded according the ROTO-UTP protocol. Here, spheroids appear comparably
126 soft during the cutting after fixation in glutaraldehyde. In fact, samples’ hardness increased after
127 the incubation with osmium tetroxide and thus the spheroids acquire resistance to cutting
128 especially after the treatment with TCH (step 3).

129 It is known that the tannic acid used after glutaraldehyde and osmium tetroxide fixation improves
130 the preservation of the cell features against shrinkage and thermal damage occurring during the
131 sample preparation^[22]. Here, when the tannic acid was added, the spheroids surface became fragile
132 during the cutting (step 4) and at the outside part of the spheroid several cells collapsed (see
133 **Supplementary Information S1**). After the embedding in Spurr’s resin, spheroids became more
134 resistant by comparing them to the other spheroids sliced in previous steps and intact during the
135 sectioning procedure (step 5), especially after the final polymerization (step 6). The size of the
136 whole spheroid was not s appreciably affected during the ROTO-UTP protocol as shown in **Figure**

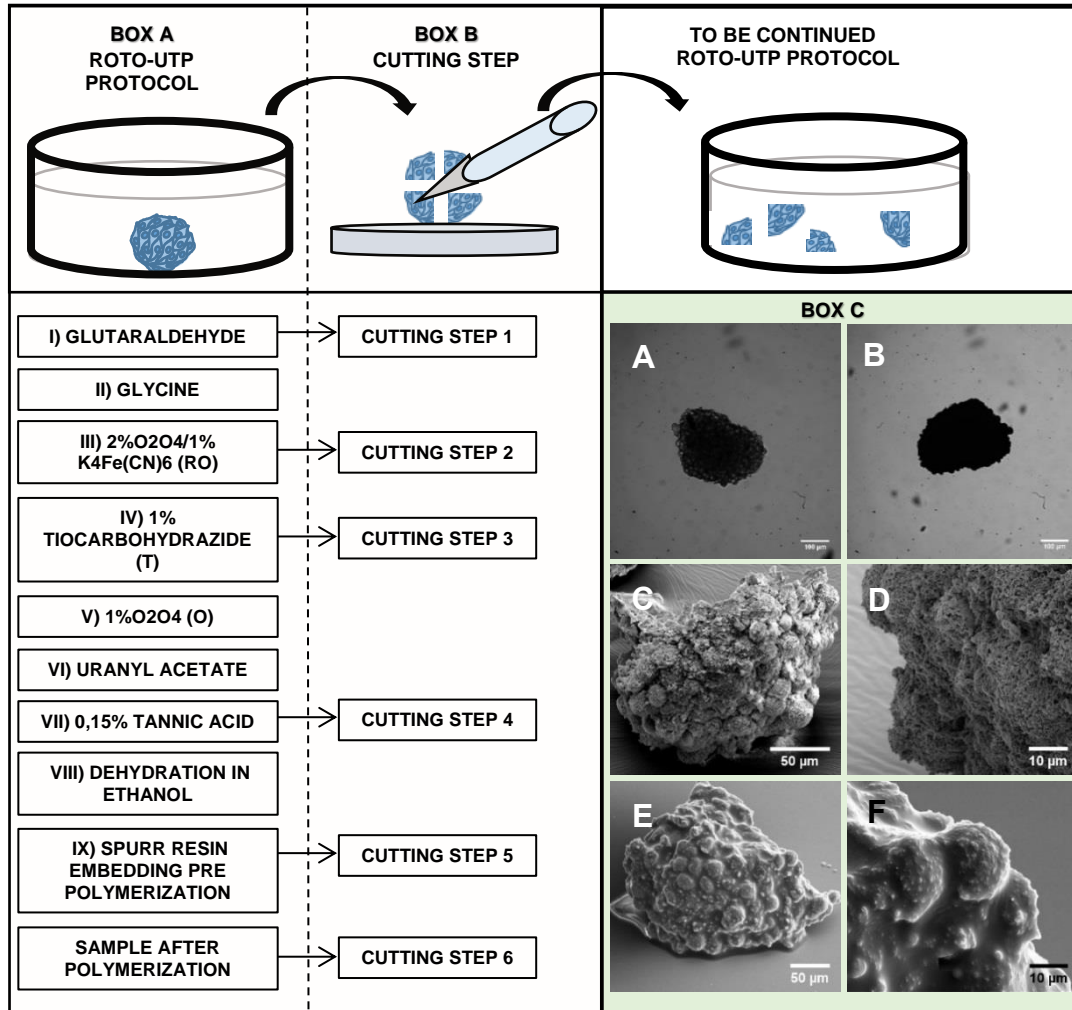
137 **2A** (post glutaraldehyde fixation) and **Figure 2B** (in Spurr's resin embedding) and further
138 discussed in see **Supplementary Information S1**).

139 Complementarily, the dehydration procedure through critical point drying (CPD) was carried out
140 on whole spheroids as shown in **Figure 2 C,D**. During the CPD process, the most crucial step is
141 in the final part of the procedure where the outflow of the gas of the supercritical carbon dioxide
142 is carried out slowly in order to avoid the collapse of samples. (0.05 bar/sec).

143 Effectively, U87-based spheroids exhibited a complex 3D structure which expands over several
144 hundreds of micrometers. Furthermore, the overall morphology have been investigated by
145 secondary electrons detection after the drying procedures. Interestingly, spheroids prepared *via*
146 CPD had individual cell bodies which appeared round and homogenously distributed throughout
147 the whole spheroid area with no comparable collapsed regions. Here, at higher magnification,
148 apical microvilli protrusions are clearly visible (**Figure 2 C-D**), however, when FIB cross
149 sectioning was performed (**Supplementary Information S2**) no intact cellular ultrastructures
150 were distinguishable because of the cavities and artefacts induced by the hard drying procedure^[23].

151

152



153 **Figure 2: SCHEMATIC FLOW OF SPECIMEN PREPARATION.** Box A summarizes the
 154 main points of the ROTO-UTP protocol (from I to IX) while in Box B the steps for the mechanical
 155 sectioning of the spheroids are reported. To evaluate the U87-MG derived spheroids ultrastructure
 156 a total of 18 spheroids were prepared with this procedure and, 3 spheroids were cut in four parts
 157 by using a razor blade at each set time points. After cutting, each sliced spheroid underwent ROTO-
 158 UTP procedure. Box C shows the size of an exemplary spheroid after fixation in glutaraldehyde
 159 (A) and its final morphology in Spurr's resin by using the optical microscope (B) and scanning
 160 electron microscope (E,F). C and D are scanning electron micrographs of whole U87-MG derived
 161 spheroids acquired in secondary electrons mode after critical point drying.

162

163 In parallel, following the ROTO procedure^[16], a group of intact spheroids was embedded in Spurr's
 164 resin. To reveal the structure of spheroids, the resin excess was removed from their surface by

165 washing with absolute ethanol for 3 seconds before the polymerization in oven at 70°C (**Figure**
166 **2E,F**).

167 In this way, the resin penetrates the intracellular domain and allows for stabilization of the
168 ultrastructures. In fact, the 3D architecture of the spheroids is preserved and the cells' cluster is
169 clearly distinguishable. However, the final removal procedure might induce a nanometer thick
170 layer of polymerized resin around the cellular bodies which covers features, i.e. microvilli, which
171 are otherwise not visible in the spheroids prepared by CPD.

172 To reveal the inner architecture of the mechanically-sectioned spheroids, FIB milling was further
173 performed on the resin-embedded specimens. First, a region of interest (ROI) was located and
174 preserved by a platinum (Pt) layer deposited *via* ion beam. In some cases, depending on the
175 geometry of the spheroid, a thick layer of gold (~ 50 nm) was deposited prior to the SEM
176 observation and was appropriate to limit charging effects and preserve the ROI. This is in fact
177 valid for smaller spheroids whose mechanical-cut subsections would have a final diameter of about
178 100-200 μm .

179 For larger subsections, first a thin film of platinum (~0.2 μm) was deposited with an electron
180 current of 26 nA and a voltage of 30 kV covering a nominal rectangular area of 75 μm by 40 μm
181 (see **Experimental Procedure** and **Supplementary Information S3**). Subsequently, an ion-
182 assisted Pt deposition was performed with an current of 9.3 nA and a voltage of 30 kV, in order to
183 achieve a final Pt thickness of ~ 1 μm . Moreover, thicker and more irregular spheroid subsections
184 were covered with an additional Pt layer of ~ 0.2 μm .

185 Then, a first large area trench out is performed to remove the material in the surrounding of the
186 ROI.

187 A rectangular area of 75 μm by 40 μm was located, and the milling was performed with a current
188 of 21 nA at 30 kV, fixing a nominal (for silicon) etching depth of 10 μm . Depending on the
189 structural composition of the spheroid subsections, the resulting cross section could be directly
190 visualized by the backscattered electrons (BSE) detector, while an additional polishing step is
191 carried out to reduce possible curtaining effect or material re-deposition^[24]. We found that at least
192 three subsequent polishing steps at decreasing currents and milling areas gave the best results in
193 terms of smoothness and definition of the target cross section. In fact, we carried out serial-
194 sequential milling steps by fixing currents at 0.79 nA, 21 nA, 93 nA, for areas of 75 μm by 30 μm ,

195 75 μm by 20 μm , 75 μm by 10 μm , respectively. The overall FIB cross section milling workflow
196 is summarized in **Supplementary Information S3**.

197 The ROI visualization was finally achieved through the BSE detector and secondary electron
198 modes (SE, see also **Supplementary Information S4**). However, BSE micrographs allow for high
199 resolution (~ 5 nm, different acquisition currents/voltages have been tested as shown in
200 **Supplementary Information S5**) and high contrast, enlightening areas with different material
201 composition, density and conductivity within the spheroid.

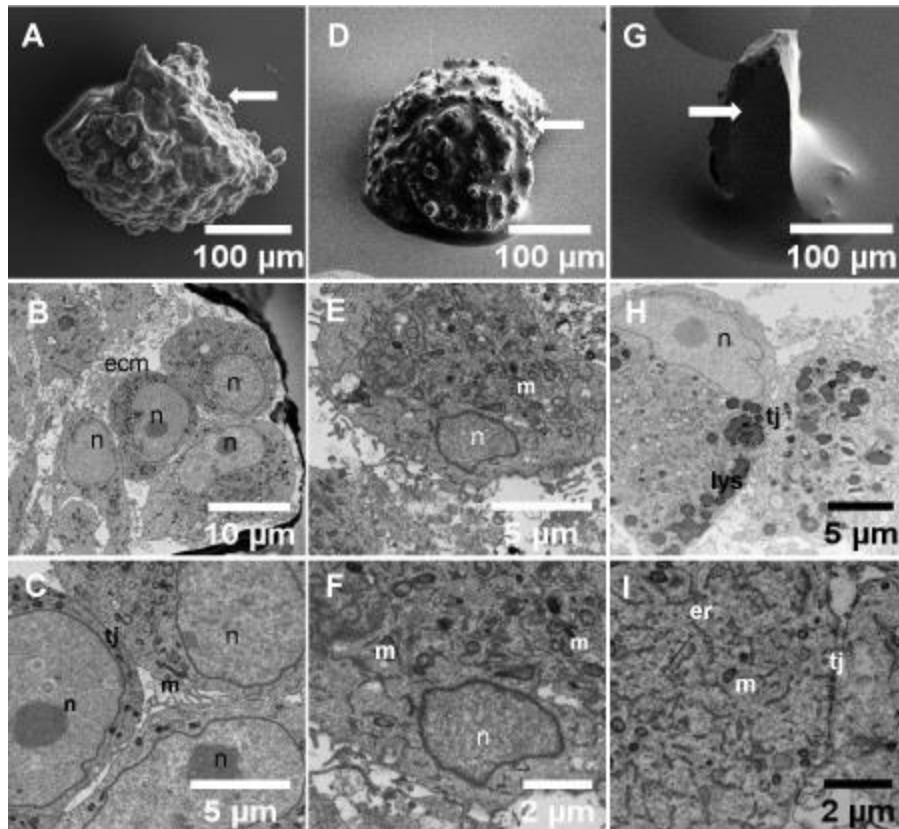
202 Here, by visualizing several cross sections, we can investigate the effect of the mechanical
203 sectioning at different steps of the staining/embedding procedure. In **Figure 3** are reported the
204 internal structure of spheroids after fixation in glutaraldehyde (step 1, **Figure 3A-C**), and in
205 Spurr's resin embedding before (**Figure 3D-F**) and after polymerization (**Figure 3G-I**) which are
206 named here as step 5 and step 6, respectively. SE micrographs in **Figure 3A,D,G** show an overview
207 of a spheroid subsection where an exemplary cutting plane is identified (white arrows). Analogous
208 micrographs have been also reported in **Supplementary Information S6-S7** and a set of
209 sequential cross sections at a 20 nm pitch have been also collected to visualize a volume of interest
210 (**Supplementary Movie 1**).

211 Furthermore, the BSE micrographs in **Figure 3** (see also **Supplementary Information S7**)
212 revealed defined nuclei (N), large number of mitochondria (M) with appreciable crests, abundant
213 rough endoplasmic reticulum (rER), extracellular matrix (EC) and tight junctions (TJ). No
214 appreciable vacuoles or similar structures, which would indicate the eradication of organelles due
215 to cutting were detectable^[25].

216 Comparing the inner and outer area of spheroids, we found evidence of compression effects due
217 to mechanical stress as effect of the mechanical cutting when spheroids underwent only primary
218 fixation (step 1).

219

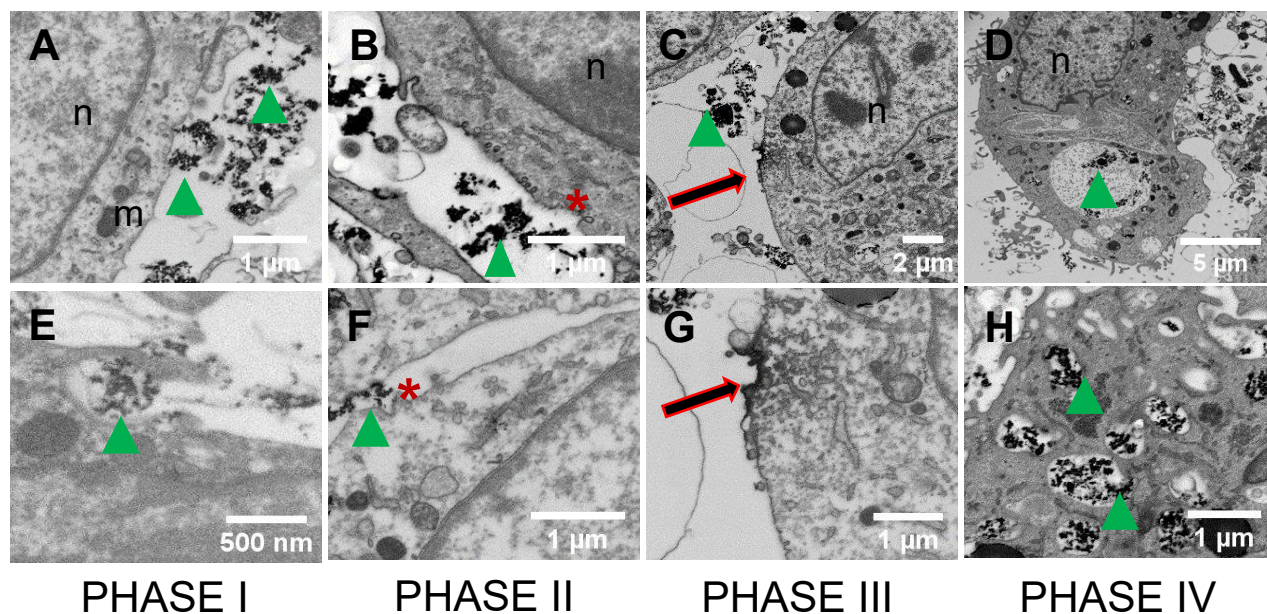
220



221
 222 **Figure 3: Characterization of spheroid subsections.** A-C) Scanning electron micrographs (BSE)
 223 of U87-MG derived spheroids prepared with ROTO and UTP protocol and resulting cross sections
 224 post glutaraldehyde cutting D-F) pre-polymerization cutting, G-I) post-polymerization cutting.

225 Spheroids subsections obtained after resin embedding prior to polymerization (step 6) were further
 226 milled and polished as mentioned earlier.

227 Finally, we investigated the interface between LMNVs and the outer and inner domains of the
 228 tumoral spheroids. The micrographs in **Figure 4E-H** display the different phases occurred during
 229 the endocytosis of LMNVs. *Phase I* represents the first contact between the nanovectors and the
 230 outer membrane (contact) followed by the formation of membrane invaginations (*phase II*) and
 231 then the formation of specific (electron-dense^[26]) clathrin-coated pits (*phase III*). **Figure 4H** shows
 232 the final LMNVs internalization and their inclusion into vesicles (*phase IV*). In particular, high
 233 magnification micrographs revealed the presence of nanovectors in the extracellular matrix
 234 domain, in the cytoplasm and incorporated in vacuoles (see **Supplementary Information S8**).



236 **Figure 4: Investigation of nanovectors uptake in spheroids by SEM-FIB.** A-H) SEM
 237 micrographs of U87-MG derived spheroids treated with ROTO-UTP protocol after incubation with
 238 lipid magnetic nanovectors: backscattered electrons micrographs on inner spheroid cross sections
 239 which exhibit diverse nanovectors uptake: phase I- contact; phase II: invagination; phase III:
 240 clathrin; phase IV: internalization. N: nuclei, green arrow: LMNVs; black arrow: clathrin; V:
 241 vacuoles, red star: invagination.

242

243 **Conclusions**

244 We showed a procedure for the investigation of 3D tumoral spheroids loaded with lipid magnetic
 245 nanovectors. Here, the resolution of the interface allows for the characterization of the cell-
 246 nanocarries interaction and the different uptake phases taking place within the spheroid. In order
 247 to proceed with localized milling and high resolution imaging, the 3D spheroids have been first
 248 mechanically sectioned. The sectioning has been performed at different steps during the heavy-
 249 metal staining and the embedding procedure and possible shear stress effects have been evaluated
 250 by performing FIB-SEM milling and imaging. Furthermore, we could investigate the cell-cell and
 251 cell-extracellular matrix interplay with nanometer resolution and, finally, evaluate the interaction
 252 between 3D spheroids and lipid magnetic nanovectors. In conclusion, this study proves a fast
 253 artefact-free processing for the nanoscale investigation of 3D complex cellular systems like

254 spheroids and organoids with nano and macromaterials which more and more are being developed
255 for tissue engineering, bioelectronic and diagnostic platforms.

256

257 **Experimental Section**

258 **Spheroids culture.** Cancer spheroids were obtained from glioblastoma multiforme U87-MG cell
259 line (ATCC® HTB-141TM). The composition of the cell medium was Dulbecco Modified Eagle's
260 Medium (DMEM) supplemented with fetal bovine serum (FBS; 10%), L-glutamine (1%), sodium
261 pyruvate (1%), non-essential amino acids (1%), penicillin (100 IU/ml), streptomycin (100 µg/ml).
262 U87 MG cells were cultured in 75 cm² flasks with a 20-85 % confluence range. For obtaining the
263 spheroids with the hanging drop method^[27], cells were treated with trypsin (0.05% for 5 minutes),
264 centrifuged (300 RCF for 6 minutes) and then resuspended at 10⁶ cells/ml concentration.
265 Subsequently, 25 µl drops of cell suspension were deposited upside down on lids of 10 cm diameter
266 Petri dishes and incubated at for 24 hours at 37°C, 5% CO₂ and 100% humidity. The obtained 2D
267 cells aggregates were finally transferred to non-adherent supports consisting in 1% agarose-coated
268 Petri dishes and cultured for 4 days with complete medium for obtaining 3D spheroids.

269 **Fluorescence imaging.** For fluorescence labelling and confocal fluorescence microscopy
270 imaging, spheroids were transferred from Petri dishes to 24-well Ibidi®, washed three times with
271 PBS, fixed with 4% paraformaldehyde (PFA) in PBS for 20 minutes at 4°C, labelled with TRITC-
272 phalloidin (100 µM) and Hoechst 33342 (1 µg ml⁻¹). Imaging was carried out with a confocal
273 fluorescence microscopy (C2s system, Nikon) and 3D reconstruction of z-stacks was performed
274 by using NIS Element software (Nikon).

275 **Nanoparticle loading.** Lipid magnetic nanovectors (LMNVs) were fabricated as previously
276 described^[7], and spheroids were incubated for 24-48 hours with 167 µg/ml of LMNVs.

277 **Fixation and staining for EM.** The specimens were prepared following the ultra-thin
278 plasticization (UTP) procedure previously described^[17,28]. Spheroids were washed once with 0.1
279 M sodium cacodylate buffer (EMS, pH 7.2) and then fixed in 2.5% glutaraldehyde solution
280 (Electron Microscopy Sciences, EMS) in the same buffer overnight at 4°C. After washing three
281 times with 0.1 M sodium cacodylate buffer, sample were post fixed in 2% osmium tetroxide/1%
282 potassium ferrocyanide (EMS, RO step), for 1 hour at 4°C in the dark and washed with buffer on
283 ice. Then spheroids were washed with distilled water and kept in water until room temperature
284 was reached. In the meantime, 1% thiocarbohydrazide solution (TCH, EMS) was prepared by

285 mixing the compound powder and distilled water and heated up at 60°C for 1 hour before filtration.
286 Samples were incubated in TCH solution at room temperature for 20 minutes in the dark (T step)
287 rinsed 3 times with distilled water and post-fixed in 1% osmium tetroxide (O step) for 1 hour at
288 room temperature. After washing with distilled water, they were finally transferred in 0.5% uranyl
289 acetate aqueous solution (EMS) overnight at 4°C in the dark. The next day, spheroids were washed
290 in chilled water and incubated for 3 minutes in 0.15% tannic acid solution (Sigma Aldrich). After
291 washing with water at 4°C, samples were dehydrated in ascending series of ethyl alcohol (Carlo
292 Erba reagents, 30%-50%-70%-95%-100%). Each step was performed for 10 minutes at 4°C. 95%
293 EtOH was performed two times while absolute ethanol step was performed two times at 4°C and
294 for a last time 10 minutes at room temperature. For the sectioning of the spheroids, a razor blade
295 with 30° micro knife (EMS) was used.

296 **Critical point drying.** After dehydration, samples were finally prepared for critical point drying
297 (CPD) During the CPD sample preparation, spheroids were placed in a critical point chamber (EM
298 CPD 300, Leica) keeping the level of ethanol to completely immerse the specimens. Then, ethanol
299 was slowly exchanged with liquid CO₂ at 15 °C and 25 cycles of fluid exchange were performed.
300 The heating up process to generate supercritical CO₂ was carried out at 37°C. Starting from 31°C,
301 the supercritical CO₂ turns in to gaseous CO₂. The gas CO₂ is then let out of the chamber through
302 a dedicated valve.

303 **Resin embedding.** Spheroids were embedded in epoxy resin (ER) according to the ultra-thin
304 plasticization protocol^[16,29] after the dehydration step. The embedding was carried out by
305 exchanging 100% ethanol solution with a mixture of absolute ethanol/Spurr's resin (EMS) with
306 the following ratios and duration: 3:1 for 2 hours; 2:1 for 2 hours; 1:1 overnight; 1:2 for 2 hours;
307 1:3 for 2 hours. Finally, the mixture was replaced with absolute resin in which spheroids were
308 incubated for one night. Sample were finally embedded in fresh Spurr's two times (3 hours per
309 each step) before polymerization. To avoid damages to the spheroid structure, a glass capillary
310 with a sealed tip was used to collect them from resin and move them to round glass coverslip. Each
311 coverslip was kept in vertical position for 2-3 hours to allow for the excess resin to drain. After
312 the polymerization at 70°C for 24 hours, samples were mounted on a 12 mm aluminum stub using
313 conductive silver paste (RS Company).

314 **SEM/FIB.** Samples were covered with a 10-20 nm-thick gold layer *via* sputter coating.
315 Afterwards, they were loaded into a dual beam machine (Helios 650, Thermo Fisher Scientific).

316 The spheroid surface was scanned with the electron beam at a voltage of 3-5 kV (secondary
317 electrons) to identify a region of interest (ROI).

318 Once a ROI was located, a first 0.2 μm -thick platinum layer was deposited *via* electron beam-
319 assisted deposition by setting a voltage at 3kV and a current in the range 0.79-9.3 nA. Afterwards,
320 the sample was tilted at 52° to be perpendicular to the ion beam and a second layer of Pt was
321 deposited by ion beam-assisted deposition to reach a final thickness of ~1 μm (in some cases a
322 deposition of an additional 200 nm thick Pt layer was necessary) .

323 A rectangular-shaped area was located for the milling. Here, the length was always kept at 75 μm
324 while the width varied (depending on the milling step, see **Supplementary Information S4**) in
325 the range 40 – 10 μm and the etching depth was nominally (as for silicon) 10 μm . The ion milling
326 was carried out fixing a voltage at 30 kV and a current in the range of 65 nA-80 pA.

327 Furthermore, possible curtaining effects and material re-deposition were compensated through
328 milling with lower currents (from 80 pA to 0.23 nA).

329 Image acquisition was performed in backscattered electrons mode fixing the dwell time at 30 μs ,
330 2 kV as voltage and 0.23 – 0.69 nA as current (dynamic focus built-in function turned on).

331

332 **References**

- 333 [1] “Spheroid-based drug screen: considerations and practical approach | Nature Protocols,” can
334 be found under <https://www.nature.com/articles/nprot.2008.226>, **n.d.**
- 335 [2] M. Zanoni, F. Piccinini, C. Arienti, A. Zamagni, S. Santi, R. Polico, A. Bevilacqua, A. Tesei,
336 *Scientific Reports* **2016**, *6*, 19103.
- 337 [3] “3D tumor spheroids as in vitro models to mimic in vivo human solid tumors resistance to
338 therapeutic drugs - Nunes - 2019 - Biotechnology and Bioengineering - Wiley Online
339 Library,” can be found under <https://onlinelibrary.wiley.com/doi/10.1002/bit.26845>, **n.d.**
- 340 [4] E. C. Costa, A. F. Moreira, D. de Melo-Diogo, V. M. Gaspar, M. P. Carvalho, I. J. Correia,
341 *Biotechnol. Adv.* **2016**, *34*, 1427.
- 342 [5] A. Marino, A. Camponovo, A. Degl’Innocenti, M. Bartolucci, C. Tapeinos, C. Martinelli, D.
343 D. Pasquale, F. Santoro, V. Mollo, S. Arai, M. Suzuki, Y. Harada, A. Petretto, G. Ciofani,
344 *Nanoscale* **2019**, *11*, 21227.
- 345 [6] K. Maier-Hauff, F. Ulrich, D. Nestler, H. Niehoff, P. Wust, B. Thiesen, H. Orawa, V.
346 Budach, A. Jordan, *J Neurooncol* **2011**, *103*, 317.
- 347 [7] C. Tapeinos, A. Marino, M. Battaglini, S. Migliorin, R. Brescia, A. Scarpellini, C. D. J.
348 Fernández, M. Prato, F. Drago, G. Ciofani, *Nanoscale* **2018**, *11*, 72.
- 349 [8] F. Pampaloni, N. Ansari, E. H. K. Stelzer, *Cell Tissue Res* **2013**, *352*, 161.
- 350 [9] K. König, A. Uchugonova, E. Gorjup, *Microscopy Research and Technique* **2011**, *74*, 9.
- 351 [10] B. K. Hoffpauir, B. A. Pope, G. A. Spirou, *Nat Protoc* **2007**, *2*, 9.
- 352 [11] K. M. Harris, E. Perry, J. Bourne, M. Feinberg, L. Ostroff, J. Hurlburt, *J. Neurosci.* **2006**,
353 *26*, 12101.

- 354 [12] J. Jaros, M. Petrov, M. Tesarova, A. Hampl, in *3D Cell Culture: Methods and Protocols*
355 (Ed.: Z. Koledova), Springer New York, New York, NY, **2017**, pp. 417–431.
- 356 [13] C. Kizilyaprak, A. G. Bittermann, J. Daraspe, B. M. Humbel, *Methods Mol. Biol.* **2014**,
357 *1117*, 541.
- 358 [14] L. H. P. Hekking, M. N. Lebbink, D. a. M. D. Winter, C. T. W. M. Schneijdenberg, C. M.
359 Brand, B. M. Humbel, A. J. Verkleij, J. A. Post, *Journal of Microscopy* **2009**, *235*, 336.
- 360 [15] K. Narayan, S. Subramaniam, *Nature Methods* **2015**, *12*, 1021.
- 361 [16] X. Li, L. Matino, W. Zhang, L. Klausen, A. F. McGuire, C. Lubrano, W. Zhao, F.
362 Santoro, B. Cui, *Nature Protocols* **2019**, *14*, 1772.
- 363 [17] D. Iandolo, F. A. Pennacchio, V. Mollo, D. Rossi, D. Dannhauser, B. Cui, R. M. Owens,
364 F. Santoro, *Advanced Biosystems* **2019**, *3*, 1800103.
- 365 [18] A. Friedmann, A. Hoess, A. Cismak, A. Heilmann, *Acta Biomaterialia* **2011**, *7*, 2499.
- 366 [19] S. Gopal, C. Chiappini, J. P. K. Armstrong, Q. Chen, A. Serio, C.-C. Hsu, C. Meinert, T.
367 J. Klein, D. W. Hutmacher, S. Rothery, M. M. Stevens, *Advanced Materials* **2019**, *31*,
368 1900488.
- 369 [20] H. E. J. Armer, G. Mariggi, K. M. Y. Png, C. Genoud, A. G. Monteith, A. J. Bushby, H.
370 Gerhardt, L. M. Collinson, *PLoS ONE* **2009**, *4*, e7716.
- 371 [21] A. J. Bushby, K. M. Y. P'ng, R. D. Young, C. Pinali, C. Knupp, A. J. Quantock, *Nat.*
372 *Protocols* **2011**, *6*, 845.
- 373 [22] T. Katsumoto, T. Naguro, A. Iino, A. Takagi, *J Electron Microsc (Tokyo)* **1981**, *30*, 177.
- 374 [23] M. Lindroth, P. B. Bell, B. A. Fredriksson, *J Microsc* **1988**, *151*, 103.
- 375 [24] F. Santoro, E. Neumann, G. Panaitov, A. Offenhäusser, *Microelectronic Engineering*
376 **2014**, *124*, 17.
- 377 [25] M. Winey, J. B. Meehl, E. T. O'Toole, T. H. Giddings, *Mol. Biol. Cell* **2014**, *25*, 319.
- 378 [26] S. Gopal, C. Chiappini, J. Penders, V. Leonardo, H. Seong, S. Rothery, Y. Korchev, A.
379 Shevchuk, M. M. Stevens, *Adv. Mater. Weinheim* **2019**, *31*, e1806788.
- 380 [27] D. Del Duca, T. Werbowetski, R. F. Del Maestro, *J. Neurooncol.* **2004**, *67*, 295.
- 381 [28] F. A. Pennacchio, F. Caliendo, G. Iaccarino, A. Langella, V. Siciliano, F. Santoro, *Nano*
382 *Lett.* **2019**, *19*, 5118.
- 383 [29] F. Santoro, W. Zhao, L.-M. Joubert, L. Duan, J. Schnitker, Y. van de Burgt, H.-Y. Lou,
384 B. Liu, A. Salleo, L. Cui, Y. Cui, B. Cui, *ACS Nano* **2017**, *11*, 8320.
- 385

386 **Acknowledgements**

387 The authors thank Laura Matino for the help with the UTP procedure and the staff of the
388 Cleanroom Facility at the Central Lab of Istituto Italiano di Tecnologia for the use of the dual-
389 beam microscope.

390

391

392 **Probing the ultrastructure of spheroids and their uptake of**
393 **magnetic nanoparticles by FIB-SEM**

394 Valentina Mollo^{1±}, Paola Scognamiglio^{1±}, Attilio Marino², Gianni Ciofani^{2,3}, Francesca Santoro^{1*}

395

396 ¹Center for Advanced Biomaterials for Healthcare, Istituto Italiano di Tecnologia, Naples, Italy.

397 ²Smart Bio-Interfaces, Istituto Italiano di Tecnologia, Pontedera, Italy.

398 ³Department of Mechanical and Aerospace Engineering, Politecnico di Torino, Torino, Italy.

399

400

401

402

403

404

405 **SUPPLEMENTARY INFORMATION**

406

407

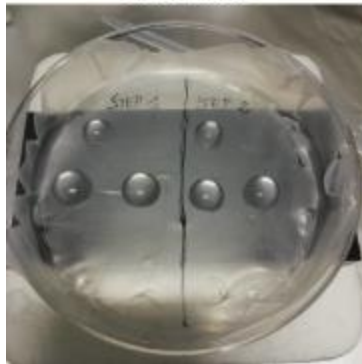
408 **Supplementary Movie 1:** sequential cross sectioning of a resin embedded spheroid (mechanical
409 cutting performed after resin infiltration) was carried out. 50 frames with a 20 nm pitch were
410 collected. The video is assembled with a speed of 4 frames/sec.

411

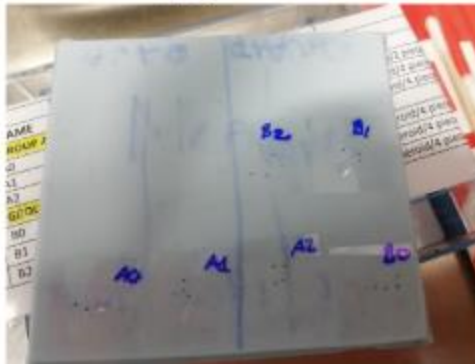
412 **S1 -Technical information concerning cutting steps of spheroids.**

413 Spheroids were divided in to four parts using a razor blade with an orientation of 30°. The
414 procedure was carried out under chemical hood with a stereo-microscope. For the cutting,
415 spheroids were put on a black support on ice to optimize their visualization and keep them
416 refrigerated at the same time. After that, all the ROTO and dehydration steps were carried out in
417 drops laid on Parafilm and the pieces of spheroids were picked up in a minimum volume (2-5 µl).
418 The cutting carried out after the primary fixation (step 1) is challenging because the spheroids are
419 soft and quite transparent. After staining with osmium tetroxide and potassium ferrocyanide both
420 handling and visualization became easier, thanks to the contrast conferred by osmium and at the
421 same time the chemical substance makes the cellular structure more compact and stable, especially
422 the plasma membrane. During the embedding steps, spheroids subsections were placed in a
423 polypropylene vials and collected using a glass capillary with a sealed tip. Before polymerization,
424 each piece was transferred on to a 22x22 mm coverslip and placed in vertical position for 2 hours.
425 After that, the resin excess was washed out with absolute ethanol for 3 seconds, and then dried
426 with filter paper. In some cases, this wash was not necessary (depending on the size of the
427 organoid) due the low viscosity of the resin. In fact, as shown our recent work^[17], the choice of
428 resin for the embedding is a crucial point for 3D specimen embedding. All coverslips with
429 spheroids were collected on a silicon mold and put in the oven for the polymerization process at
430 70°C overnight. In order to evaluate the possible volume change of spheroids during the ROTO-
431 UTP protocol, a group of 12 intact spheroids prepared with the aforementioned protocol. At the
432 each cutting step, brightfield imaging (16X magnification) was performed and the total area of the
433 spheroid was calculated. As shown in the graph, there are no relevant differences in the spheroids'
434 area across all steps of the ROTO protocol.

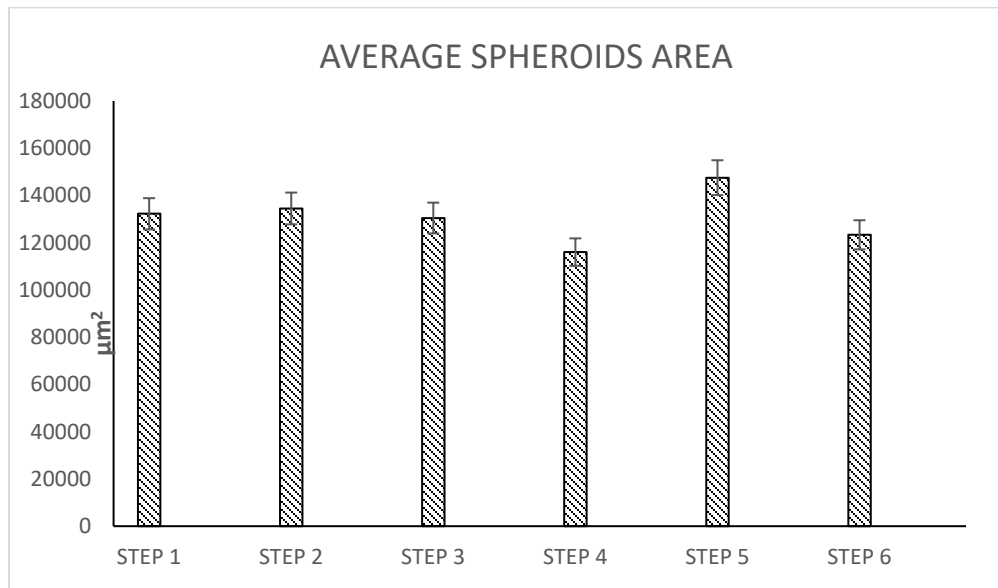
Incubation/washing pieces of spheroids



Pieces of spheroids after polymerization



435

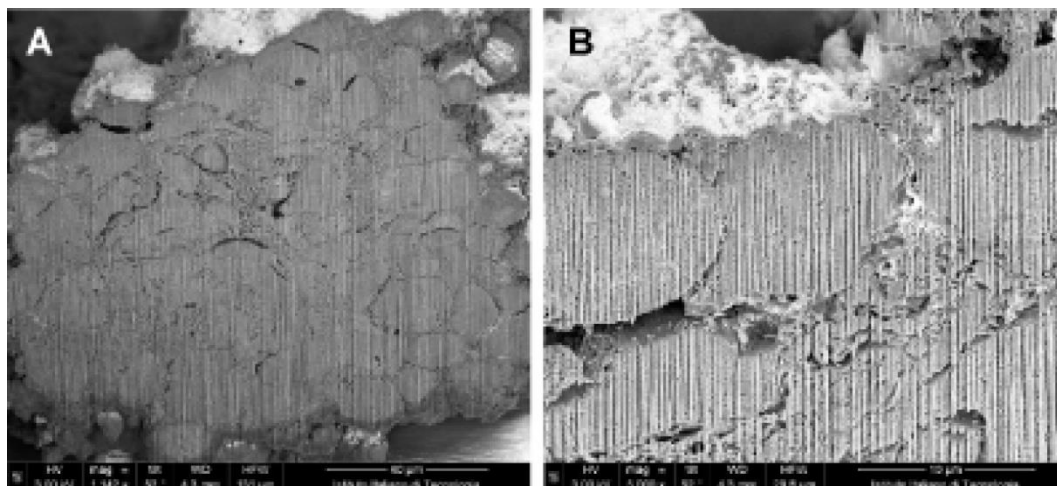


436

437

438 **S2-FIB cross sectioning of a spheroid dehydrated *via* CPD.**

439 At an initial observation cells seem to preserve their shapes showing no difference in their external
440 morphology. However, after the FIB milling (**Figure S2-A**) the intracellular domain has a sponge-
441 like structure and no ultrastructures are distinguishable.

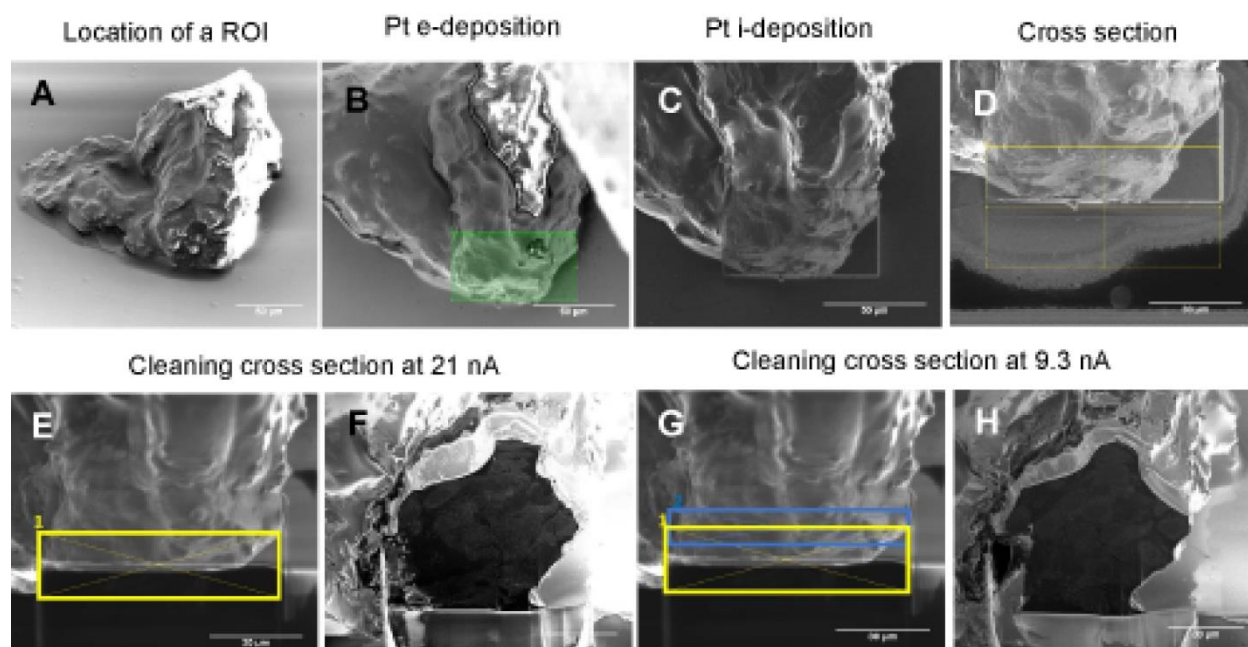


442

443 **Figure S2 :** Scanning electron micrographs of FIB cross sections of CPD specimens.

444

445 **S3 – FIB cross sectioning procedure.**



446

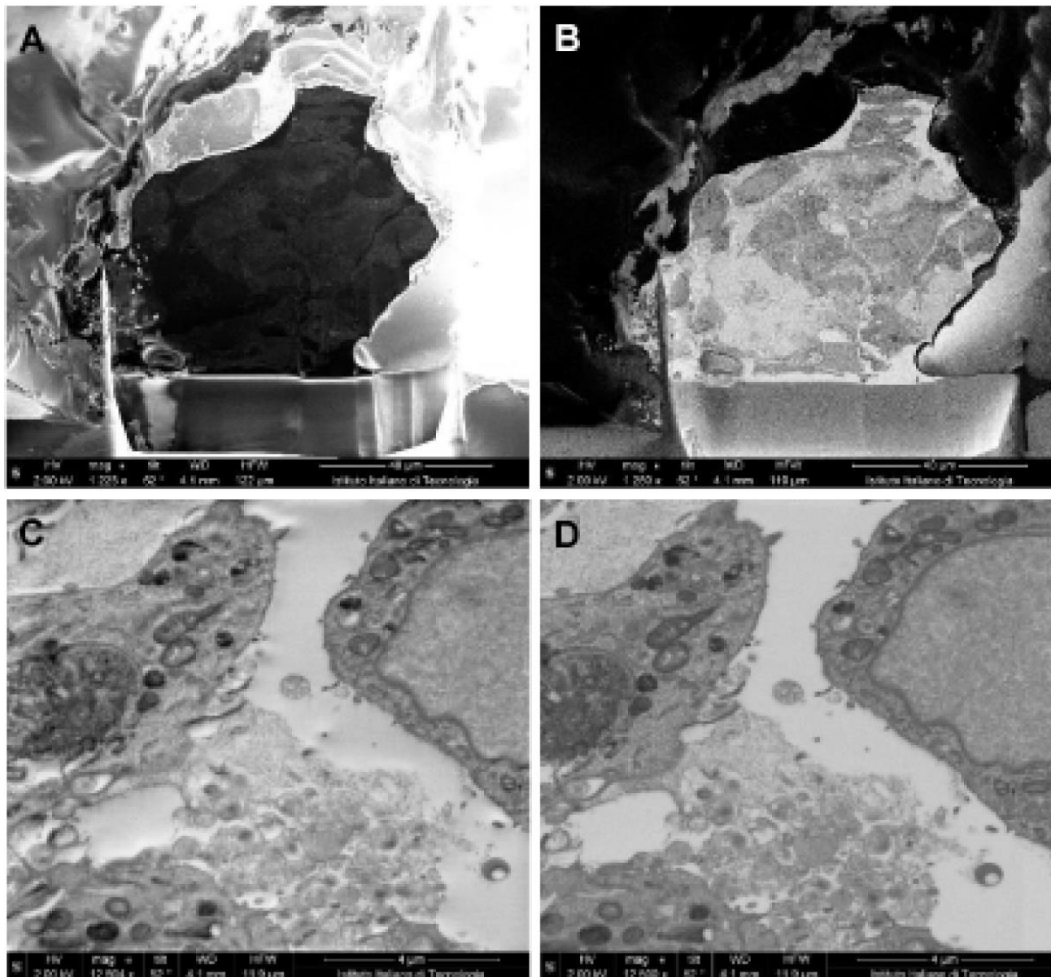
447

448 **Figure S3:** A) location of region of interest (ROI), B) deposition of Pt layer is a rectangular ROI
 449 of 75 μm by 40 μm (electron beam assisted) C) Pt ion-beam assisted deposition (area of 75 μm
 450 by 40 μm), D) ion beam milling, E-F) polishing at 21 nA, G-H) polishing at 9.3 nA.

451

452 **S4- Imaging by secondary and backscattered electrons detection.**

453 Secondary electrons are very sensitive to the surface of the material and give mainly information
454 its 3D morphology (**Figure S4-C**). Instead, backscattered electrons possess higher energy than
455 secondary electrons thus they are sensitive to the composition of the specimen. Here, the quality
456 of the images depends on the presence of heavy atoms; an area characterized by heavy atoms
457 structures appears bright in the backscattered electron image (**Figure S4-B**) and the shape of
458 borders and internal organelles are clear and well defined (**Figure S4-D**).

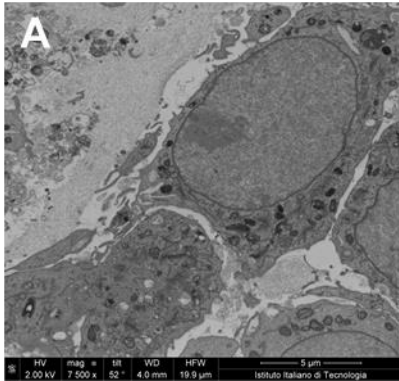


459
460 **Figure S4** : micrographs acquired with SE A&C) and BSE detectors B&D).

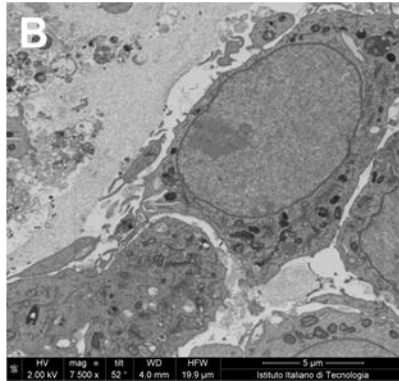
461
462 **S5 – Image resolution depending on voltage/current in backscattered electrons detection**
463 **mode.**

464 In **Figure S5**, images of the same area were acquired with the same voltage (2 kV) but increasing
465 current intensity: 0.20 nA, 0.40 nA, 0.80 nA.

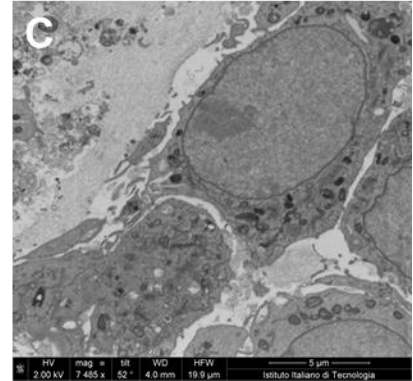
2 kV – 0.20 nA



2 kV – 0.40 nA



2 kV – 0.80 nA



466

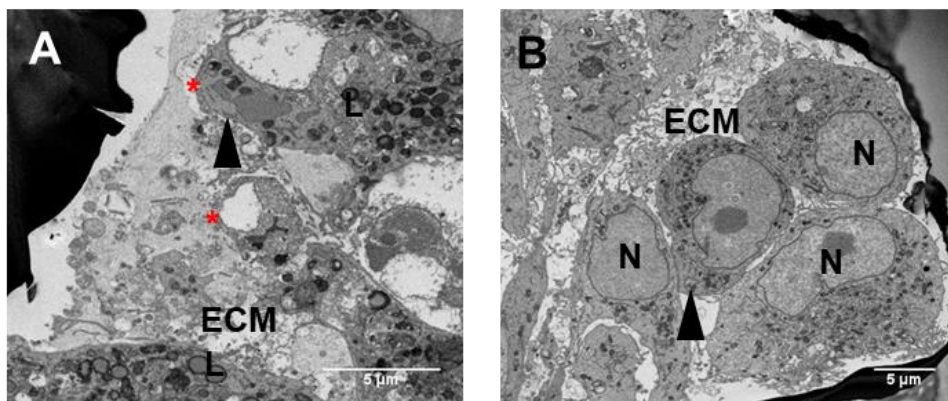
467 **Figure S5:** BSE micrographs of the same area acquired at 2 kV and currents of: A) 0.20 nA B)
468 0.40 nA C) 0.80 nA.

469

470 **S6- Investigation of ultrastructure in subsection of spheroids obtained by mechanical**
471 **sectioning after primary fixation in glutaraldehyde (STEP 1).**

472 **Figure S6-A** depicts the outer part of a spheroid while **Figure S6-B** its inner domain. There are
473 no appreciable damage in organelles or membrane. In fact nuclei, mitochondria, lysosomes, are
474 well preserved, but the cells appear compressed in their outer domains as they underwent
475 mechanical stress during the cut.

476



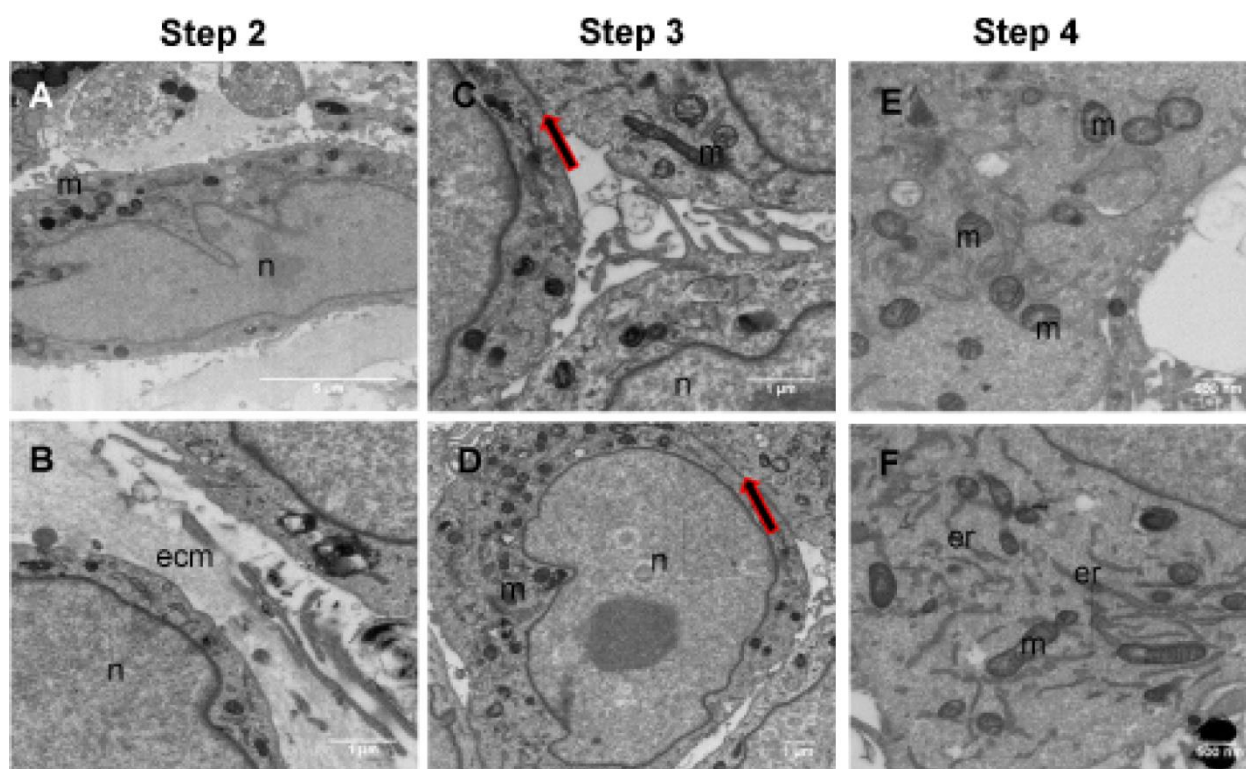
477

478 **Figure S6:** SEM-FIB cross section of U87 derived spheroids after ROTO/UTP protocols at cutting
479 step 1 (after glutaraldehyde fixation) A) external area of spheroids with evidence of cracks (red
480 star), B) inner area of spheroids. N: nuclei, ECM: extracellular matrix, L: lysosomes

481

482 **S7- Investigation of ultrastructure in subsection of spheroids obtained by mechanical**
483 **sectioning at STEP 2, STEP 3, STEP 4.**

484 To investigate the possible mechanical damage due the sectioning of spheroids, SEM/FIB cross
485 sections of tree intermediate cutting step are reported after treatment with osmium tetroxide (step
486 2), after tannic acid (step 3) and before polymerization (Step4). In all micrographs, the cell
487 ultrastructure is well preserved: the cell-cell junctions are evident, and the cytoplasmic organelles
488 are not eradicated or damaged. In fact the cytoplasm is homogenous, the plasma membrane is
489 intact, and some organelles, i.e. mitochondria or nuclei, show their peculiar morphology.

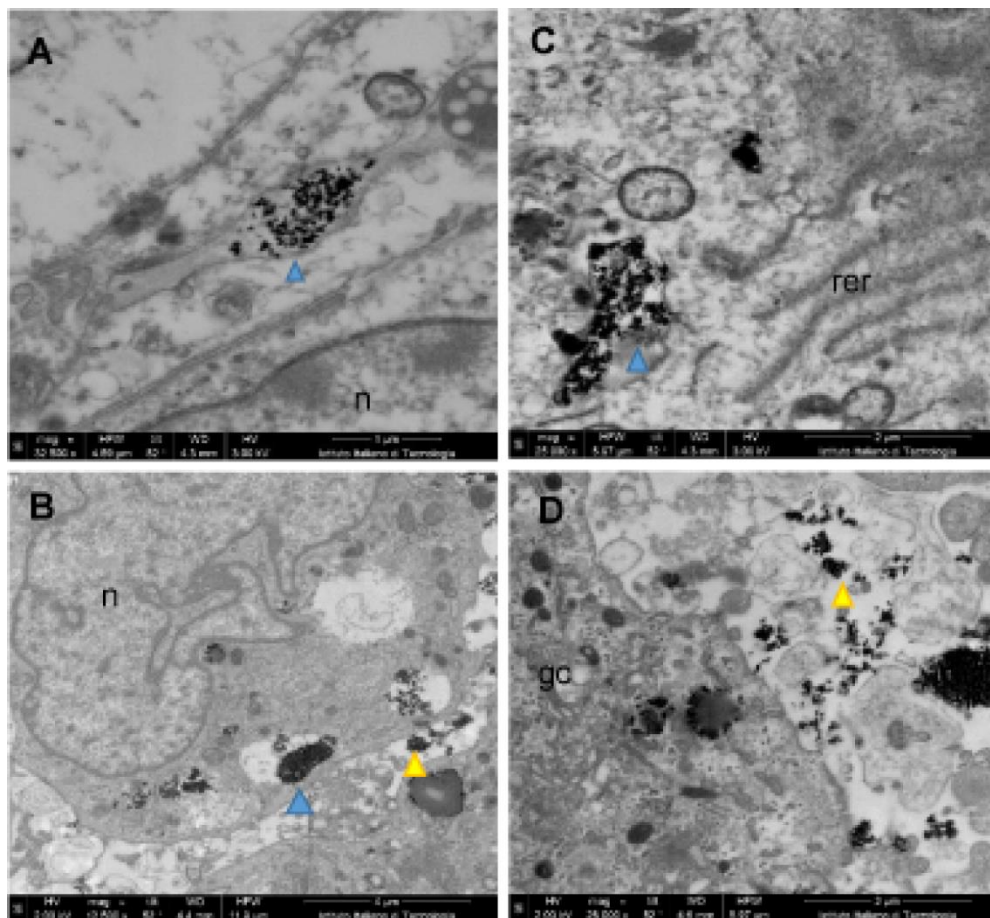


490
491 **Figure S7:**SEM-FIB cross sections of U87 spheroids treated with ROTO protocol: A,B) after
492 osmium tetroxide cutting (step2); C,D) after tannic acid cutting (Step 3); E,F) after Spurr's resin
493 embedding, before polymerization cutting (step 4). Cell-cell junctions are preserved (red/black
494 arrow), mitochondria (m) crests are definite. Also endoplasmic reticulum is well appreciable
495 (er)and extra cellular matrix is compact.

496

497 **S8- Internalization of nanovectors in to spheroids.**

498 To characterize the internalization of nanovectors at nanometric resolution, spheroids were
499 incubated with LMNVs. SEM/FIB cross section were acquired and the spheroid/nanovector
500 interface was investigated. As shown in **Figure S8**, LMNVs are internalized through endocytosis
501 in vesicles or vacuoles (blu arrows); nanovectors are also found free in cytoplasm (yellow arrow).
502



503
504 **Figure S8:** U87 derived spheroids after ROTO and UTO protocol previously incubated with
505 LMNVs. Nanovectors are detected in vacuoles (blu arrow) inside the cell and/or free in cytoplasm
506 (yellow arrows) n: nuclei, gc: Golgi complex, rer: rough endoplasmic reticulum.